Available online at www.sciencedirect.com
ScienceDirect
Journal of Solid State Chemistry 181 (2008) 14–19
JOURNAL OF SOLID STATE CHEMISTRY
www.elsevier.com/locate/jssc

An investigation of structural parameters and magnetic and optical properties of EuLn_2Q_4 (Ln = Tb–Lu, Q = S, Se)

Geng Bang Jin[a], Eun Sang Choi[b], Robert P. Guertin[c], Thomas E. Albrecht-Schmitt[a,*]

[a]*Department of Chemistry and Biochemistry and Center for Actinide Science, Auburn University, Auburn, AL 36849, USA*
[b]*Department of Physics and National High Magnetic Field Laboratory, Florida State University, Tallahassee, FL 32310, USA*
[c]*Department of Physics and Astronomy, Tufts University, Medford, MA 02155, USA*

Received 19 September 2007; received in revised form 15 October 2007; accepted 22 October 2007
Available online 5 November 2007

Abstract

EuLn_2Q_4 (Ln = Tb–Lu; Q = S, Se) has been synthesized using Sb_2Q_3 (Q = S, Se) fluxes at 1000 °C. These compounds crystallize in a $CaFe_2O_4$-type three-dimensional channel structure that is built from edge-shared double rutile chains of [LnQ_6] octahedra running down the *b*-axis. Each double chain is connected at the vertices to four other double chains to form open channels where bicapped trigonal prismatic Eu^{2+} ions reside. All of these compounds show antiferromagnetic ordering with Neel temperatures, T_N~3–4 K. The optical band gaps for $EuTb_2Se_4$, $EuDy_2Se_4$, $EuHo_2Se_4$, $EuEr_2Se_4$, $EuTm_2Se_4$, $EuYb_2Se_4$ $EuLu_2Se_4$, and $EuYb_2S_4$ are found to be 2.0, 1.8, 1.8, 1.7, 1.8, 1.3, 1.7, and 1.6 eV, respectively.

Keywords: Interlanthanide chalcogenide; Mixed-lanthanide chalcogenide; Magnetic properties of interlanthanide chalcogenides

1. Introduction

A large number of ternary compounds with a formula ALn_2Q_4, where A = Sr, Ba, Eu; Ln = La–Lu, Y, Sc; Q = O, S, Se, Te, crystallize in the $CaFe_2O_4$-type [1] structure [2–11]. These systems have been extensively studied owing to their interesting optical and magnetic properties. Some of these compounds are potential IR window materials [7]. SrLn_2O_4 (Ln = Dy, Ho, Er, Tm, Yb) [10] and BaLn_2O_4 (Ln = Pr, Nd, Sm–Ho) [11] with a triangle-based array of magnetic Ln ions were recently recognized as potentially geometrically frustrated systems. Compared to SrLn_2Q_4 or BaLn_2Q_4, Eu^{2+}-based phases are more magnetically interesting. Eu^{2+} cations have fairly large magnetic moments (7.94 μ_B) and potentially strong magnetic couplings between each other, which usually leads to long-range magnetic ordering [12,13]. Many EuLn_2Q_4 (Q = S, Se) compounds have been characterized by powder X-ray diffraction and magnetic measurements [3,4]. They have shown antiferromagnetic transitions, metamagnetic transitions, and ferromagnetic transitions, depending on the choice of Ln^{3+}. To our knowledge, $EuEr_2S_4$ is the only compound of the EuLn_2Q_4 (Q = S, Se) [5] series examined with single X-ray diffraction. Selenide analogs are less studied compared to EuLn_2S_4. Here we present the syntheses, single crystal structures, optical, and magnetic properties of EuLn_2Se_4 (Ln = Tb–Lu). $EuYb_2S_4$ is also included in the discussion for comparison.

2. Experimental

2.1. Starting materials

Eu (99.9%, Alfa-Aesar), Tb (99.9%, Alfa-Aesar), Dy (99.9%, Alfa-Aesar), Ho (99.9%, Alfa-Aesar), Er (99.9%, Alfa-Aesar), Tm (99.9%, Alfa-Aesar), Yb (99.9%, Alfa-Aesar), Lu (99.9%, Alfa-Aesar), Se (99.5%, Alfa-Aesar), S (99.5%, Alfa-Aesar), and Sb (99.5%, Alfa-Aesar) were used as received. The Sb_2Q_3 (Q = S, Se) fluxes were prepared from the direct reaction of the elements in sealed fused-silica ampoules at 850 °C.

*Corresponding author. Fax: +1 334 844 6959.
E-mail address: albreth@auburn.edu (T.E. Albrecht-Schmitt).

0022-4596/$ - see front matter © 2007 Elsevier Inc. All rights reserved.
doi:10.1016/j.jssc.2007.10.028

2.2. Syntheses

EuLn_2Q_4 (Ln = Tb–Lu; Q = S, Se) were obtained from the reaction of Eu, Ln, Q, and Sb_2Q_3 (Q = S, Se) in a molar ratio of 1:2:4:0.5. All of the mixtures were loaded into fused-silica ampoules in an Ar-filled glovebox. The ampoules were sealed under vacuum and heated in a programmable tube furnace using the following profile: 2 °C/min to 500 °C (held for 1 h), 0.5 °C/min to 1000 °C (held for 7 d), 0.05 °C/min to 550 °C (held for 2 d), and 0.5 °C/min to 24 °C. The products included high yields of red or black crystals of EuLn_2Q_4 and unreacted Sb_2Q_3 blocks. For EuLn_2Se_4 (Ln = Tb, Dy, Ho), the yield of desired products becomes low. Instead, there were large amounts of $EuSbSe_3$ [13] and some unidentified black microcrystalline 'EuLnSbSe' phases. EDX experiments have shown that the crystals of 'EuLnSbSe' include all four elements, but they are too small for single-crystal X-ray diffraction experiments. EuLn_2Q_4 crystals were isolated manually for physical property measurements. All of the compounds are stable in air. Powder X-ray diffraction measurements were used to confirm phase purity by comparing the powder patterns calculated from the single crystal X-ray structures with the experimental data. Semi-quantitative SEM/EDX analyses were performed using JEOL 840/Link Isis or JEOL JSM-7000F instruments. Eu, Ln, and Q percentages were calibrated against standards. Sb was not detected in the crystals. The Eu:Ln:Q ratios were determined to be approximately 1:2:4 from EDX analyses.

2.3. Crystallographic studies

Single crystals of EuLn_2Q_4 (Ln = Tb–Lu; Q = S, Se) were mounted on glass fibers with epoxy and optically aligned on a Bruker APEX single-crystal X-ray diffractometer using a digital camera. Initial intensity measurements were performed using graphite monochromated Mo$K\alpha$ ($\lambda = 0.71073$ Å) radiation from a sealed tube and a monocapillary collimator. SMART (v 5.624) was used for preliminary determination of the cell constants and data collection control. The intensities of reflections of a sphere were collected by a combination of three sets of exposures (frames). Each set had a different ϕ angle for the crystal and each exposure covered a range of 0.3° in ω. A total of 1800 frames were collected with exposure times per frame of 10 or 20 s depending on the crystal.

For EuLn_2Q_4 (Ln = Tb–Lu; Q = S, Se), determinations of integrated intensities and global refinement were performed with the Bruker SAINT (v 6.02) software package using a narrow-frame integration algorithm. These data were treated first with a face-index numerical absorption correction using XPREP [14], followed by a semi-empirical absorption correction using SADABS [15]. The program suite SHELXTL (v 6.12) was used for space group determination (XPREP), direct methods structure solution (XS), and least-squares refinement (XL) [14]. The final refinements included anisotropic displacement parameters for all atoms and secondary extinction. Some crystallographic details are given in Table 1. As an example, atomic coordinates and equivalent isotropic displacement parameters for $EuYb_2S_4$ are given in Table 2. Additional crystallographic details can be found in the Supporting Information. Further details of the crystal structure investigation may be obtained from the Fachinformationzentrum Karlsruhe, D-76344 Eggenstein-Leopoldshafen, Germany (fax: +49 7247 808 666; Email: crysdata@fiz-karlsruhe.de) on quoting the depository numbers CSD 418588, 418589, 418590, 418591, 418592, 418593, 418594, and 418595.

Table 1
Crystallographic data for EuLn_2Q_4 (Ln = Tb–Lu; Q = S, Se)

Formula	$EuTb_2Se_4$	$EuDy_2Se_4$	$EuHo_2Se_4$	$EuEr_2Se_4$	$EuTm_2Se_4$	$EuYb_2Se_4$	$EuLu_2Se_4$	$EuYb_2S_4$
F_w	785.64	792.80	797.66	802.32	805.66	813.88	817.74	626.28
Color	Red	Red	Red	Red	Red	Black	Red	Dark red
Crystal system	Orthorhombic	Orthorhombic	Orthorhombic	Orthorhombic	Orthorhombic	Orthorhombic	Orthorhombic	Orthorhombic
Space group	*Pnma* (no. 62)	*Pnma* (no. 62)	*Pnma* (no. 62)	*Pnma* (no. 62)	*Pnma* (no. 62)	*Pnma* (no. 62)	*Pnma* (no. 62)	*Pnma* (no. 62)
a (Å)	12.429(2)	12.442(1)	12.4258(7)	12.4066(7)	12.3874(8)	12.3591(9)	12.3489(9)	11.809(1)
b (Å)	4.1413(5)	4.1224(3)	4.1027(2)	4.0864(2)	4.0737(3)	4.0612(3)	4.0470(3)	3.9194(3)
c (Å)	14.915(2)	14.866(1)	14.8096(8)	14.7596(8)	14.7119(9)	14.664(1)	14.6174(1)	14.086(1)
V (Å^3)	767.7(3)	762.5(2)	755.0(1)	748.3(1)	742.4(1)	736.0(2)	730.5(2)	651.9(2)
Z	4	4	4	4	4	4	4	4
T (K)	193	193	193	193	193	193	193	193
λ (Å)	0.71073	0.71073	0.71073	0.71073	0.71073	0.71073	0.71073	0.71073
ρ_{calcd} (g cm^{-3})	6.797	6.906	7.018	7.122	7.208	7.345	7.435	6.381
μ (cm^{-1})	451.43	465.00	481.28	498.42	515.30	532.82	551.06	391.00
R (F)[a]	0.0304	0.0298	0.0219	0.0214	0.0248	0.0211	0.0190	0.0208
R_w (F_o^2)[b]	0.0656	0.0667	0.0490	0.0501	0.0606	0.0512	0.0448	0.0471

[a] $R(F) = \sum||F_o| - |F_c|| / \sum|F_o|$
[b] $R_w(F_o^2) = \left[\sum\left[w(F_o^2 - F_c^2)^2\right] / \sum wF_o^4\right]^{1/2}$.

Table 2
Atomic coordinates and equivalent isotropic displacement parameters for $EuYb_2S_4$

Atom (site)	x	y	z	U_{eq} (Å^2)[a]
Eu	0.75797(4)	$\frac{1}{4}$	0.66230(3)	0.0083(1)
Yb1	0.41916(3)	$\frac{1}{4}$	0.10025(2)	0.0078(1)
Yb2	0.43311(3)	$\frac{1}{4}$	0.61031(3)	0.0088(1)
S1	0.2080(2)	$\frac{1}{4}$	0.1735(2)	0.0086(4)
S2	0.1293(2)	$\frac{1}{4}$	0.4729(1)	0.0071(4)
S3	0.5226(2)	$\frac{1}{4}$	0.7841(2)	0.0094(4)
S4	0.4131(2)	$\frac{1}{4}$	0.4219(2)	0.0075(4)

[a] U_{eq} is defined as one-third of the trace of the orthogonalized U_{ij} tensor.

2.4. Powder X-ray diffraction

Powder X-ray diffraction patterns were collected with a Rigaku Miniflex powder X-ray diffractometer using Cu$K\alpha$ ($\lambda = 1.54056$ Å) radiation.

2.5. Magnetic susceptibility measurements

Magnetism data were measured on powders obtained from ground crystals in gelcap sample holders with a Quantum Design MPMS 7T magnetometer/susceptometer between 2 and 300 K and in applied fields up to 7 T. DC susceptibility measurements were made under zero-field-cooled conditions with an applied field of 0.1 T. Susceptibility values were corrected for the sample diamagnetic contribution according to Pascal's constants [16] as well as for the sample holder diamagnetism. θ_p values were obtained from extrapolation fits between 100 and 300 K.

2.6. UV–vis–NIR diffuse reflectance spectroscopy

The diffuse reflectance spectra for $EuLn_2Q_4$ (Ln = Tb–Lu; Q = S, Se) in the form of ground powders were measured from 200 to 2500 nm using a Shimadzu UV3100 spectrophotometer equipped with an integrating sphere attachment. The Kubelka–Munk function was used to convert diffuse reflectance data to absorption spectra [17].

3. Results and discussion

3.1. Crystal structures

The $EuLn_2Q_4$ (Ln = Tb–Lu; Q = S, Se) compounds adopt the $CaFe_2O_4$-type [1] three-dimensional channel structure, which has been detailed in other references [5–11]. These compounds crystallize in an orthorhombic system with a space group of *Pnma*. As shown in Fig. 1, the structure includes one crystallographically unique bicapped trigonal prismatic Eu^{2+} position and two octahedral Ln^{3+} sites. [LnQ_6] octahedra share edges with identical units

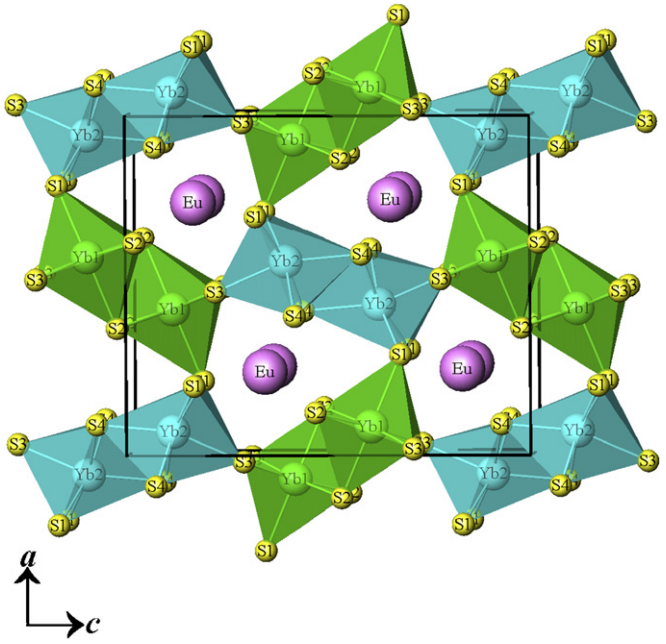

Fig. 1. A view of the three-dimensional channel structure of $EuYb_2S_4$ down the *b*-axis.

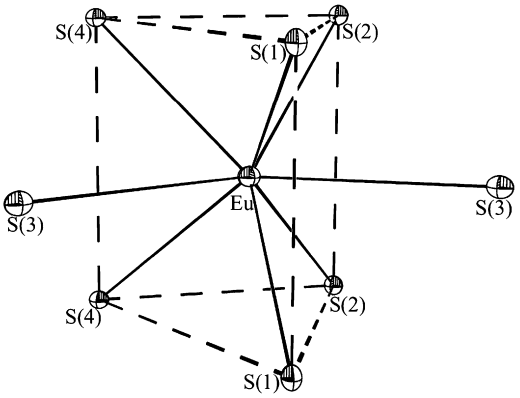

Fig. 2. Illustrations of the coordination environment for Eu ions in $EuYb_2S_4$.

both in the direction of chain propagation (the *b*-axis) and with adjacent chains to form double rutile chains. Each double chain is connected at the vertices to four other double chains to build open channels where Eu^{2+} ions reside. The coordination environment of Eu^{2+} ions is displayed in Fig. 2. Selected bond distances (Å) for $EuLn_2Q_4$ are listed in Table 3. Eu–Q distances are in the range of 3.1469(7) and 3.438(2) Å for selenides, and 3.039(2) and 3.266(2) Å for the sulfide. They are comparable to Shannon's values for eight-coordinated Eu^{2+} ions [18]. Bond distances for [$LnSe_6$] octahedra are normal as well.

The unit cell volumes and Eu–Eu distances (*b*-axis) are plotted as a function of choice of Ln^{3+} in Fig. 3. These values decrease linearly with increasing atomic number because of the lanthanide contraction.

Table 3
Selected bond distances (Å) for EuLn_2Q_4 (Ln = Tb–Lu; Q = S, Se)

Formula	$EuTb_2Se_4$	$EuDy_2Se_4$	$EuHo_2Se_4$	$EuEr_2Se_4$	$EuTm_2Se_4$	$EuYb_2Se_4$	$EuLu_2Se_4$	$EuYb_2S_4$
Eu–Q(1) × 2	3.176(1)	3.176(1)	3.1747(7)	3.1740(8)	3.1754(9)	3.1701(8)	3.1730(7)	3.058(2)
Eu–Q(2) × 2	3.183(1)	3.177(1)	3.1670(7)	3.1616(7)	3.1571(9)	3.1506(7)	3.1469(7)	3.039(2)
Eu–Q(3)	3.380(2)	3.392(1)	3.3933(9)	3.388(1)	3.377(1)	3.367(1)	3.3501(9)	3.215(2)
Eu–Q(3)	3.438(2)	3.419(1)	3.4024(9)	3.391(1)	3.387(1)	3.379(1)	3.3823(9)	3.266(2)
Eu–Q(4) × 2	3.204(1)	3.205(1)	3.1980(7)	3.1945(7)	3.1920(9)	3.1848(7)	3.1831(7)	3.054(2)
Ln(1)– Q(1)	2.870(1)	2.864(1)	2.8566(8)	2.8458(9)	2.838(1)	2.8256(9)	2.8196(8)	2.699(2)
Ln(1)–Q(2) × 2	2.8955(9)	2.8794(9)	2.8643(6)	2.8500(7)	2.8368(8)	2.8267(6)	2.8132(6)	2.718(1)
Ln(1)–Q(2)	2.872(1)	2.858(1)	2.8413(8)	2.8280(9)	2.817(1)	2.8042(9)	2.7944(8)	2.687(2)
Ln(1)–Q(3) × 2	2.8012(9)	2.7940(9)	2.7812(6)	2.7722(6)	2.7643(7)	2.7551(6)	2.7473(6)	2.640(1)
Ln(2)–Q(1) × 2	2.884(1)	2.8753(9)	2.8636(6)	2.8531(7)	2.8428(8)	2.8356(6)	2.8242(6)	2.722(2)
Ln(2)–Q(3)	2.837(1)	2.819(1)	2.8082(8)	2.7959(9)	2.786(1)	2.7751(9)	2.7653(8)	2.666(2)
Ln(2)–Q(4) × 2	2.878(1)	2.8680(8)	2.8532(6)	2.8410(6)	2.8304(7)	2.8229(6)	2.8112(6)	2.710(1)
Ln(2)–Q(4)	2.839(1)	2.826(1)	2.8163(8)	2.803(1)	2.788(1)	2.777(1)	2.7658(9)	2.665(2)

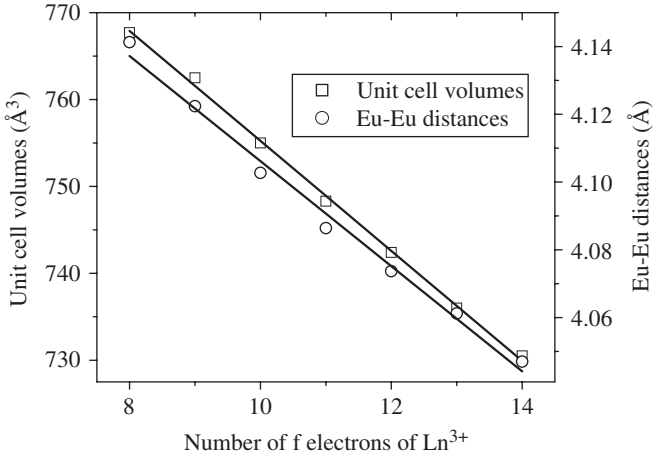

Fig. 3. Unit cell volumes (Å^3) and Eu–Eu distances (Å) vs. the number of f electrons of Ln^{3+} for EuLn_2Se_4 (Ln = Tb–Lu).

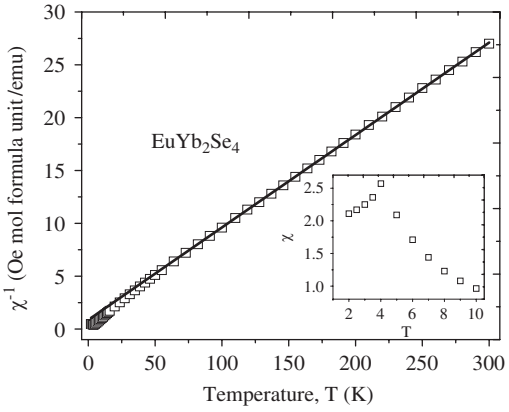

Fig. 4. Temperature dependence of the reciprocal molar magnetic susceptibility for $EuYb_2Se_4$ under an applied magnetic field of 0.1 T between 2 and 300 K. The straight line represents the fit to the Curie–Weiss law in the range of 100–300 K. Inset shows the molar magnetic susceptibility at low temperature.

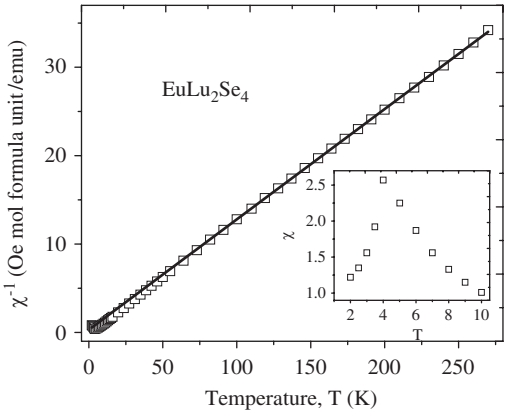

Fig. 5. Inverse molar magnetic susceptibility vs. temperature for $EuLu_2Se_4$ under an applied magnetic field of 0.1 T between 2 and 300 K. The solid line represents the fit to the Curie–Weiss law in the range of 100–300 K. Inset shows the molar magnetic susceptibility at low temperature.

3.2. Magnetic properties

Magnetic susceptibilities of EuLn_2Q_4 (Ln = Tb–Lu; Q = S, Se) have been measured on powder samples. Only the data for $EuYb_2Se_4$ and $EuLu_2Se_4$ are shown in Figs. 4 and 5. The magnetic behavior of other materials can be found in the Supporting Information (Figs. S1–S6). All of these compounds except $EuEr_2Se_4$ and $EuHo_2Se_4$ exhibit a similar transition below 5 K, which is relatively independent of the choice of Ln^{3+}. The transitions for $EuEr_2Se_4$ and $EuHo_2Se_4$ are anomalous, as both samples show a sharp antiferromagnetic transition on a large background of Curie-like Er or Ho paramagnetism. The transitions show no divergence in zero-field-cooled vs. field-cooled measurements, so they are ascribed to signify conventional antiferromagnetic ordering. As mentioned earlier, the triangular characteristics of the Ln^{3+} sublattice suppress the potential long-range ordering of the Ln^{3+} ions [10,11], even though this effect is expected to be less significant in sulfides and selenides than in oxides. In addition, T_N for $EuLu_2Se_4$ is nearly identical to that of $EuYb_2Se_4$ and $EuTm_2Se_4$, and Lu^{3+} ions carry no moment. However, there is a weak inverse correlation between the Eu^{2+}-generated antiferromagnetic transition temperature and the total angular momentum quantum number of the Ln^{3+}

ion. Clearly the observed magnetic ordering in these materials is due to the Eu^{2+} ions. The Eu–Eu coupling is brought about by Eu–*Q*–Eu superexchange that is also exemplified by antiferromagnetic Eu_3O_4 [19], which has a somewhat similar crystal structure.

The high-temperature susceptibilities of EuLn_2Q_4 obey the Curie–Weiss law. Deviations can be found for most of these compounds at relatively low temperatures caused by a crystal-field splitting of the ground state for the Ln^{3+} cations. (Crystal field splitting effects will be negligible for Eu^{2+} ions, as the ground-state angular momentum quantum number for Eu^{2+} is $J = S = 7/2$, thus with no orbital contribution.) Table 4 lists the magnetic parameters for EuLn_2Q_4, which were obtained from fitting the data in the range of 100–300 K with the Curie–Weiss law. The experimental effective magnetic moments are all close to that expected for full moments of the free Eu^{2+} and Ln^{3+} ions [20]. Weiss temperatures (θ_p) are all negative, which is consistent with antiferromagnetic interactions between magnetic ions. Detailed magnetic properties including the hydrostatic pressure dependence of the antiferromagnetic ordering temperatures are discussed in another paper [21].

3.3. Optical properties

EuLn_2Q_4 (Ln = Tb–Lu; Q = S, Se) possess different colors. EuLn_2Se_4 (Ln = Tb, Dy, Ho, Er, Tm, Lu) are red. $EuYb_2S_4$ is dark red and $EuYb_2Se_4$ is black. The UV–vis–NIR diffuse reflectance spectra of EuLn_2Q_4 are presented in Fig. 6. The band gaps of $EuTb_2Se_4$, $EuDy_2Se_4$, $EuHo_2Se_4$, $EuEr_2Se_4$, $EuTm_2Se_4$, $EuYb_2Se_4$, $EuLu_2Se_4$, and $EuYb_2S_4$ are found to be 2.0, 1.8, 1.8, 1.7, 1.8, 1.3, 1.7, and 1.6 eV, respectively. These values are consistent with observed colors. $EuYb_2Se_4$ has a much smaller gap than that of other selenides. In addition, $EuTm_2S_4$ and $EuLu_2S_4$, prepared by the same method, have the same colors and similar band gaps as their selenide analogs [22]. These unusual results conflict with the conventional scheme of the band gap for sulfides and selenides, which is the gap between the valence band of 3*p*/4*p* states of S/Se and the conduction band of 5*d* (6*s*) states of Ln^{3+} cations [23,24]. Choices of Q should play a more important role than Ln^{3+} ions for the band gap values of EuLn_2Q_4. In contrast, the band gap for $EuYb_2S_4$ is larger than the value of $EuYb_2Se_4$ because of the lower energy of 3*p* states of S. The band gap structures of Yb-based compounds appear to be different from the rest of the compositions. Future work including theoretical calculations for their electronic structures may help to clear up this mystery. The fine structure observed in the spectra for $EuDy_2Se_4$ and $EuTm_2Se_4$ is due to *f*–*f* transitions within the lanthanide ions. There is some tailing below the initial absorption edge for $EuDy_2Se_4$, $EuEr_2Se_4$, $EuTm_2Se_4$, $EuYb_2Se_4$, and $EuLu_2Se_4$, indicating the presence of a low-level impurity (Sb_2Se_3) or indirect band gaps for these materials.

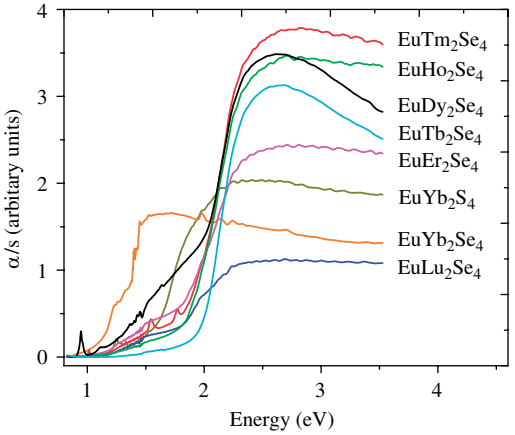

Fig. 6. UV–vis–NIR diffuse reflectance spectra of EuLn_2Q_4 (Ln = Tb–Lu; Q = S, Se).

Table 4
Magnetic parameters for EuLn_2Q_4 (Ln = Tb–Lu; Q = S, Se)

Formula	P_{cal} (μ_B)[a]	P_{eff} (μ_B)[a]	θ_p (K)[b]	R^2	T_N (K)
$EuTb_2Se_4$	15.87	16.44(2)	−12.9(6)	0.99984	3.6
$EuDy_2Se_4$	17.00	16.315(6)	−3.8(1)	0.99999	3.0
$EuHo_2Se_4$	16.96	16.46(2)	−2.7(5)	0.99988	3.2
$EuEr_2Se_4$	15.72	15.519(8)	−6.1(2)	0.99998	4.0
$EuTm_2Se_4$	13.33	13.35(1)	−7.2(4)	0.99992	4.0
$EuYb_2Se_4$	10.21	9.563(8)	−9.9(4)	0.99994	4.3
$EuLu_2Se_4$	7.94	8.00(1)	−2.4(5)	0.9999	4.4
$EuYb_2S_4$	10.21	8.76(1)	−11.0(5)	0.99989	4.3

[a] P_{cal} and P_{eff}: calculated [19] and experimental effective magnetic moments per formula unit.
[b] Weiss constant (θ_p) and goodness of fit (R^2) obtained from high-temperature (100–300 K) data.

4. Conclusions

EuLn_2Q_4 (Ln = Tb–Lu; Q = S, Se) were prepared using Sb_2Q_3 (Q = S, Se) fluxes and characterized by single-crystal X-ray diffraction, magnetic susceptibility measurements, and UV–vis–NIR diffuse reflectance spectroscopy. This isotypic series adopts the $CaFe_2O_4$-type three-dimensional channel structure. All of these compounds are antiferromagnets at low temperature due to the magnetic couplings between Eu^{2+} ions. EuLn_2Q_4 are semiconductors and some of them have atypical band gaps.

Acknowledgments

This work was supported by the US Department of Energy under Grant DE-FG02-02ER45963 through the EPSCoR Program. Funds for purchasing the UV–vis–NIR spectrometer used in these studies were provided through the Chemical Sciences, Geosciences and Biosciences Division, Office of Basic Energy Sciences, Office of Science, Heavy Elements Program, US Department of Energy, under Grant DE-FG02-01ER15187. E.S.C. acknowledges support from NSF-DMR 0203532. A portion of this work was performed at the National High Magnetic Field Laboratory, which is supported by the National Science

Foundation Cooperative Agreement no. DMR-0084173, by the State of Florida, and by the Department of Energy.

Appendix A. Supplementary materials

Supplementary data associated with this article can be found in the online version at doi:10.1016/j.jssc.2007.10.028.

References

[1] D.F. Becker, J.S. Kasper, Acta Crystallogr. 10 (1957) 332.
[2] P.J. Flahaut, M. Guittard, M. Patrie, M.P. Pardo, S.M. Golabi, L. Domange, Acta Crystallogr. 19 (1965) 14.
[3] F. Hulliger, O. Vogt, Phys. Lett. 21 (1966) 138.
[4] W. Lugscheider, H. Pink, K. Weber, W. Zinn, Z. Angew. Phys. 30 (1970) 36.
[5] P. Lemoine, D. Carre, M. Guittard, Acta Crystallogr. C 41 (1985) 667.
[6] J.D. Carpenter, S.-J. Hwu, Acta Crystallogr. C 48 (1992) 1164.
[7] C.K. Lowe-Ma, T.A. Vanderah, J. Solid State Chem. 117 (1995) 363.
[8] A.A. Narducci, Y.T. Yang, M.A. Digman, A.B. Sipes, J.A. Ibers, J. Alloys Compd. 303 (2000) 432.
[9] I. Felner, Y. Yeshurun, G. Hilscher, T. Holubar, G. Schaudy, U. Yaron, O. Cohen, Y. Wolfus, E.R. Yacoby, L. Klein, F.H. Potter, C.S. Rastomjee, R.G. Egdell, Phys. Rev. B 46 (1992) 9132.
[10] H. Karunadasa, Q. Huang, B.G. Ueland, J.W. Lynn, P. Schiffer, K.A. Regan, R.J. Cava, Phys. Rev. B 71 (2005) 144414.
[11] Y. Doi, W. Nakamori, Y. Hinatsu, J. Phys.: Condens. Matter 18 (2006) 333.
[12] G.B. Jin, D.M. Wells, S.J. Crerar, T.C. Shehee, A. Mar, T.E. Albrecht-Schmitt, Acta Crystallogr. E 61 (2005) i116.
[13] G.B. Jin, S.J. Crerar, A. Mar, T.E. Albrecht-Schmitt, J. Solid State Chem. 179 (2006) 1596.
[14] G.M. Sheldrick, SHELXTL PC, Version 6.12, An Integrated System for Solving, Refining, and Displaying Crystal Structures from Diffraction Data, Siemens Analytical X-ray Instruments, Inc., Madison, WI, 2001.
[15] G.M. Sheldrick, Acta Crystallogr. A51 (1995) 33.
[16] L.N. Mulay, E.A. Boudreaux, Theory and Applications of Molecular Diamagnetism, Wiley-Interscience, New York, 1976.
[17] W.W. Wendlandt, H.G. Hecht, Reflectance Spectroscopy, Interscience Publishers, New York, 1966.
[18] R.D. Shannon, Acta Crystallogr. A32 (1976) 751.
[19] L. Holmes, M. Schieber, Phys. Rev. 167 (1968) 440.
[20] C. Kittel, Introduction to Solid State Physics, sixth ed., Wiley, New York, 1986.
[21] R.P. Guertin, E.S. Choi, G.B. Jin, T.E. Albrecht-Schmitt, J. Appl. Phys., in press.
[22] G.B. Jin, T.E. Albrecht-Schmitt, unpublished results.
[23] A.V. Prokofiev, A.I. Shelykh, A.V. Golubkov, I.A. Smirnov, J. Alloys Compd. 219 (1995) 172.
[24] A.V. Prokofiev, A.I. Shelykh, B.T. Melekh, J. Alloys Compd. 242 (1996) 41.